Feasibility study of quantum computing using trapped electrons

Qian Yu,[1,2,*] Alberto M. Alonso,[1,2] Jackie Caminiti,[1,2] Kristin M. Beck,[3] R. Tyler Sutherland,[4] Dietrich Leibfried,[5] Kayla J. Rodriguez,[6] Madhav Dhital,[6] Boerge Hemmerling,[6] and Hartmut Häffner[1,2,7]

[1]*Physics Department, University of California, Berkeley, California 94720, USA*
[2]*Challenge Institute for Quantum Computation, University of California, Berkeley, California 94720, USA*
[3]*Lawrence Livermore National Laboratory, 7000 East Avenue, Livermore, California 94550, USA*
[4]*Department of Electrical and Computer Engineering, Department of Physics and Astronomy, University of Texas at San Antonio, San Antonio, Texas 78249, USA*
[5]*Time and Frequency Division, National Institute of Standards and Technology, 325 Broadway, Boulder, Colorado 80305, USA*
[6]*Physics Department, University of California, Riverside, California 92521, USA*
[7]*Computational Research Division, Lawrence Berkeley National Laboratory, Berkeley, California 94720, USA*

(Received 7 December 2021; accepted 31 January 2022; published 15 February 2022)

We investigate the feasibility of using electrons in a linear Paul trap as qubits in a future quantum computer. We discuss the necessary experimental steps to realize such a device through a concrete design proposal, including trapping, cooling, electronic detection, spin readout, and single- and multiqubit gate operations. Numeric simulations indicate that two-qubit Bell-state fidelities of order 99.99% can be achieved assuming reasonable experimental parameters.

DOI: 10.1103/PhysRevA.105.022420

I. INTRODUCTION

Ongoing efforts to build a quantum computer are based on various physical implementations. One of the most established implementations is based on trapped ions in Paul traps, where qubits are encoded in the internal states of the ions' valence electrons and entangled using spin-dependent forces that couple the ions' internal states to their collective motion [1]. Trapped ions are advantageous because they exhibit coherence times exceeding 10 min [2–4] and flexible connectivity [5,6]. Also, errors per gate as low as 10^{-6} [7,8], for single-qubit gates, and 10^{-3} [9–11], for multiqubit gates, have been achieved. However, multiqubit operations between ions are typically relatively slow ($\sim$10 μs) compared to, for example, superconducting qubits ($\sim$10 ns). In addition, the optical technology required for cooling, preparation, readout, and controlling thousands of trapped ion qubits is still in its infancy [12–14].

Here, we conduct a feasibility study of trapped-electron-based quantum computing. Electrons are attractive for quantum computing because they are extremely light and a natural two-level spin system (qubit) that has a large enough magnetic moment to be manipulated with well-established microwave technology and thermal reservoirs, eliminating the need for qubit control optics. The mass reduction of four orders of magnitude, relative to trapped ions, increases the motional frequencies of the particle in the trapping potential, thereby facilitating the speed for multiqubit operations and transport. Additionally, the electrons' two-level spin structure removes certain complications of traditional atomic and solid-state qubits such as leakage of quantum information from the computational subspace, potentially making high-fidelity operations easier and simplifying quantum error correction [15]. The electrons' spin degree of freedom can be initialized, coherently controlled, and measured using gigahertz electronics, microwaves, and a low-temperature (0.4 K) reservoir, making all-electronic control feasible and thus replacing some of the optical engineering challenges required to build large-scale quantum information processing devices with trapped ions.

Quantum information processing using electrons in Penning traps has been considered before [16–18]. In addition, there are efforts under way to use electrons trapped on superfluid films of helium and neon [19–23], where single electrons have been detected and manipulated [21]. Quantum computing with electrons in Paul traps has been proposed and discussed in Refs. [24–26]. The first step towards this goal has been taken by trapping and detecting electrons in a room-temperature Paul trap [27]. Similar efforts are under way in the Noguchi group at University of Tokyo.

Here we discuss basic elements for an electron quantum computer. We study the anticipated challenges of cooling electrons, detecting their spins, and implementing multiqubit gates. Furthermore, we carry out simulations of quantum gates to determine dominant error sources.

II. PROTOTYPE

The prototype system we consider is sketched in Fig. 1 and assumed to reside in a cryogenic environment at 4 K. We chose a quadrupole configuration consisting of two layers separated by 60 μm. The approximately quadrupolar geometry, with a width of the quadrupole electrodes of 50 μm, a length

*qian_yu@berkeley.edu

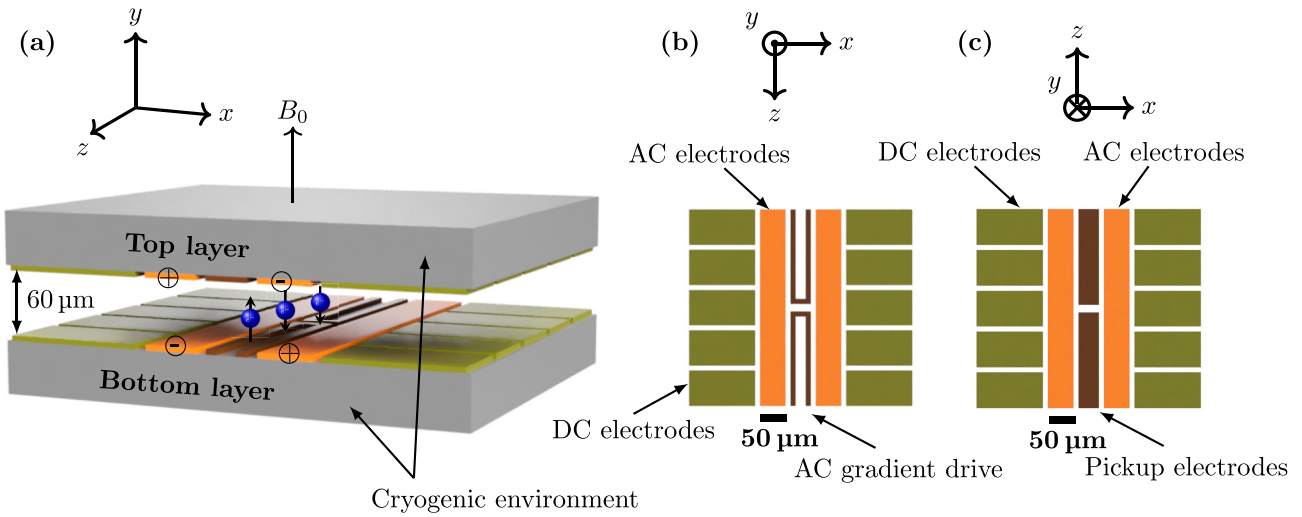

FIG. 1. (a) A prototype trap design provides a framework for analyzing the feasibility of trapped electron quantum computing. The trap consists of two substrates separated by 60 μm, supporting four AC electrodes that are driven out of phase. Driving currents through the two center electrodes of the bottom layer generates a magnetic field gradient or a homogeneous magnetic field (both along the z axis) depending on the relative phase of the currents. The two center electrodes of the top layer serve to pick up the image current generated by the electron motion. The plus and minus signs at the AC electrodes indicate the phase of the AC drive applied to each electrode. (b) Top view of the bottom substrate. (c) Bottom view of the top substrate.

of the quadrupole electrodes of 390 μm, and electrode separation of 60 μm, is efficient in generating both deep and stiff traps, and the symmetry suppresses odd orders of anharmonic terms of the trapping potential. The vast different charge-to-mass ratio for bare electrons requires a higher AC drive frequency as opposed to that used for commonly trapped ions, which can be achieved by incorporating capacitively coupled resonators to introduce microwaves to the surface-electrode prototype trap. As indicated in Fig. 1, we assume to drive the two AC electrodes in each plane out of phase with each other and opposite to the other plane with an amplitude of $U_0 =$ 14 V with a frequency of $\omega_{\rm ac} = 2\pi \times 10.6$ GHz. This yields transverse secular frequencies $\omega_{\rm t} = 2\pi \times 2$ GHz. Further, we assume an axial trap frequency of $\omega_{\rm a} = 2\pi \times 300$ MHz, produced by appropriate static (-15 to 15 V) potentials applied to the DC electrodes shown in Fig. 1. Using the pseudopotential approximation we find a trap depth of approximately 80 meV while numerical simulation of electron trajectories shows substantial losses for electrons with an initial energy above 22 meV (see Appendix D). The minimum of the trapping potential resides in the center between layers and in the middle of the electrode structure along the x and z axes.

Low-energy electrons can be introduced into the trap by ionization of a thermal atomic beam in the trapping region. This procedure enables both the creation of low-energy electrons by tuning the lasers close to the ionization threshold and *in situ* ionization near the trap center by aligning the optics. As demonstrated in Ref. [27], the loading efficiency of such a procedure is about 1 electron per 10 μs on average. The electron motion can be damped to reliably form a Coulomb crystal and detected by coupling the induced image current to a resonant cryogenic tank circuit held at 0.4 K, which creates a voltage opposing the electron motion that is dissipated over the effective resistance of the circuit until the thermal energy of the electron is equivalent to the circuit temperature. The average micromotion amplitude of a thermalized electron at $T = 0.4$ K is $x_{\rm MM} = \frac{q}{2} x_{\rm t} = 80$ nm, where $q = 0.53$ is the stability parameter in the Mathieu equation, and $x_{\rm t} = \sqrt{\frac{2k_{\rm B}T}{m_e \omega_{\rm t}^2}} \approx 0.3$ μm is the average amplitude of the transverse secular motion. Here, $k_{\rm B}$ is the Boltzmann constant and m_e is the electron mass.

Quantum information will be stored in superpositions of the spin states of the electron, denoted as $|\uparrow\rangle$ and $|\downarrow\rangle$. We assume that a homogeneous magnetic field $B_0 = 3.6$ mT along the y direction splits the degeneracy of the two spin states, leading to a frequency difference of $\omega_{\rm qubit} = 2\pi \times 100$ MHz between both logical eigenstates. The electron qubits will be manipulated with the help of the two "hairpin" electrodes between the AC electrodes of the bottom layer, labeled "AC gradient drive" in Fig. 1. The spin direction of the electrons is coupled to the electron motion by using an oscillating magnetic field gradient resonant with the electron motion to apply a spin-dependent displacement force. Measuring the phase of the resulting image current in one of the electrodes projects the spin state into one of the qubit eigenstates, as discussed in Ref. [25]. The oscillating magnetic field gradient is created by currents of opposite direction in the middle segments of the hairpin electrodes and can also be used to drive multiqubit gates. Reversing the current direction in one of the hairpin electrodes produces an oscillating homogeneous magnetic field perpendicular to the quantization axis that can drive single-qubit gates.

A. Cooling of electrons

Trapping electrons and cooling them to low temperatures to minimize the average extent of their wavefunction, thus allowing for a nondestructive spin-state readout, is essential for quantum computing with trapped electrons. The electron

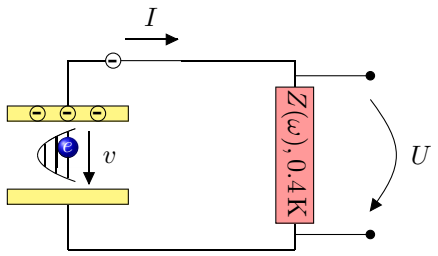

FIG. 2. A moving trapped electron induces an image current in the trap electrodes, which creates a potential difference U and is dissipated via the impedance of an attached tank circuit which is held at 0.4 K.

motion can be damped by coupling the image current induced by the electron motion to a high-impedance cryogenic tank circuit, as shown in Fig. 2. This has been demonstrated in Penning trap experiments [28]. The damping occurs because the current induced in the tank circuit by image charges from the moving electron is dissipated by the circuit's resistance, creating a voltage at the trap electrodes that opposes the electron motion until the induced current is of similar magnitude as the thermal (Johnson) current fluctuations in the circuit.

The induced current is $I = ev/d_{\text{eff}}$, where v is the velocity of the electron with charge e and d_{eff} describes the effective distance of the electrode structure [28,29]. For the y direction and the cooling circuit attached to the two center pickup electrodes on the top layer, we find $d_{\text{eff}} = 138\ \mu$m, a reduction by about a factor of 2 as compared to the ideal plate capacitor geometry. For the axial (z) direction with the cooling circuit attached to one of the top center pickup electrodes, we find $d_{\text{eff}} = 254\ \mu$m.

The cooling time constant can be derived by considering the electron as a circuit element [28]:

$$\tau = \frac{m_e}{e^2}\frac{d_{\text{eff}}^2}{\text{Re}(Z)}. \tag{1}$$

Here, $Z = Q\sqrt{L/C}$ is the on-resonance impedance of the attached circuit. Assuming that the pickup electrodes are attached to a tank circuit with a moderate quality factor of $Q = 1000$, a capacitance of $C = 1$ pF, a resonant frequency of $2\pi \times 2$ GHz, and an inductance of $L = 6$ nH results in an on-resonance impedance of $\text{Re}(Z) = 80$ kΩ. Inserting this into Eq. (1), we find a cooling time constant of 8 μs for the mode in the y direction. For the mode in the z direction, the cooling time constant is approximately 4 μs ($\omega_{\text{a}} = 2\pi \times 300$ MHz, $L = 250$ nH, $C = 1$ pF, $Q = 1000$, $Z = 500$ kΩ).

In equilibrium, the average energy of the cooled mode will be that of the temperature of the tank circuit, i.e., $\langle E\rangle = \hbar\omega_{\text{t}}(\bar{n} + 1/2) = k_{\text{B}}T_{\text{t}}$. Assuming 2 GHz for one of the transverse modes and $T_{\text{t}} = 0.4$ K, the average motional excitation will be $\bar{n} \approx 4$.

Since the vertical transverse mode can be cooled following this protocol, the horizontal transverse mode and the axial mode can also be cooled by coupling them to the vertical transverse mode. Such parametric coupling is common practice for electrons and ions in Penning traps [29] and has been demonstrated for ions in a Paul trap [30]. To achieve this, our electrode geometry allows us to generate a quadrupole field with projection overlap on a pair of modes that oscillates at the difference frequency between the two modes. This leads to an interaction that causes an energy exchange between the two motional modes. Assuming that we hold the high-frequency vertical transverse mode at 0.4 K, the low-frequency axial mode will be cooled to a temperature reduced by the frequency ratio, $T_{\text{a}} = T_{\text{t}}\omega_{\text{a}}/\omega_{\text{t}} = 60$ mK. Scaling results from Ref. [30], we expect coupling times between the two motional modes of below 1 μs.

Since resistive cooling does not affect the spin state of the qubit, the electrons can be cooled while keeping the qubits coherent, and no sympathetic coolant particles are needed to be able to perform high-fidelity operations on electron qubits. In fact, the cooling does not need to be turned off for most of the time; only during multiqubit gates where a common mode of motion is used as a bus, as well as during the spin-motion conversion process for detection, must the cooling be switched off. We also note that efficient cooling takes place only if the electron motion is on resonance with the resonant frequency of the tank circuit. Thus, we can adjust the cooling time constant by changing the trapping potential.

B. Spin readout and initialization of electrons

The spin direction can be read out by first coupling the spin to the electron motion and then measuring the phase of the motion, as discussed in Ref. [25]. In order to couple the spin direction to the motion, one can apply a magnetic field gradient oscillating at the axial motional frequency. As the direction of the force due to the magnetic field gradient depends on the spin direction, this creates a state-dependent displacement acting on the initial thermal state. The measurement result is encoded in the phase of the motion, and thus the critical requirement is to maintain the coherence of the motion. Therefore, it is important to create the displaced state faster than the motional dephasing time. Thus, one of the limiting factors is the strength of the magnetic field gradient. We calculate that passing 1 A of current through the hairpin wires in Fig. 1 will create a gradient of 120 T/m. Applying an oscillating current of this amplitude at the axial motional frequency of the electrons for 10 μs maps the spin direction to the motion with a fidelity of 99.7%, assuming an initial axial mode temperature of 60 mK, cooled via parametric coupling as described before. To increase the amplitude of the image current further to a readily measurable size, electric forces can be used to parametrically amplify the coherent state $|\alpha\rangle$ by modulating the trapping voltages at twice the trap frequency [31,32].

Since it is critical to conserve phase coherence, it is necessary to consider the harmonicity of the axial trapping potential created by the DC electrodes in Fig. 1. Experimentally one can use the potentials applied to the 20 DC electrodes to minimize anharmonicities in the axial potential. Expanding the optimized trap potential into the Taylor series $V(z) = V(0)(1 + c_2z^2 + c_4z^4 + c_6z^6)$ and $c_2 = 1\ \mu\text{m}^{-2}$, we find coefficients $c_4 = 10^{-7}\ \mu\text{m}^{-4}$ and $c_6 = -2\times10^{-9}\ \mu\text{m}^{-6}$, while odd- and higher even-order terms are negligible, assuming a typical 16-bit digital-to-analog converter. voltage uncertainty of 200 μV for each trapping voltage. From this we find the trap frequency uncertainty as $\Delta\omega_{\text{a}}/\omega_{\text{a}} \approx (3A^2c_4/4 + 15A^4c_6/16)/c_2$, where

A is the amplitude of the motion. To excite the motion above the Johnson noise at 0.4 K, the amplitude must exceed $A > 1.3\,\mu$m. At this amplitude, the relative frequency shift due to the trap anharmonicity would be only 1.2×10^{-7}, corresponding to an absolute shift of the resonance frequency of 36 Hz, which is negligible on the considered timescale of $10\,\mu$s.

The current induced by the motion of the electron produces a voltage drop across the tank circuit that can be picked up with a Johnson-noise limited amplifier. The phase of the electron motion is then encoded in the phase of the amplified voltage. Electronic detection of electrons is standard in Penning traps [29,33–35]. In Paul traps, however, the strong trap drive of ∼14 V may saturate the amplifiers, requiring careful filtering (see Appendix B).

With state readout in place, we can initialize electron spin by first measuring it and then flipping it conditioned on the measurement result. If the electron is found in the state we would like to initialize it in, nothing is done. If it is in the other state, we perform a π pulse using a microwave field.

C. Quantum gates with electrons

Single-qubit gates can be performed by using microwave pulses near the Zeeman resonance, similarly to how error rates of 10^{-6} have been achieved for ions [7]. For evaluating two-qubit gates, the Mølmer-Sørensen gate [1,36] and its controlled phase gate ($\sigma_z \otimes \sigma_z$) variant [37] are considered. While typically performed using optical-frequency radiation, it can also be implemented using static or oscillating magnetic field gradients [38–43]. The general idea is that a force oscillating nearly resonant with a mode frequency of the two-electron crystal excites the motion if the force on the individual electrons has the correct symmetry. For the phase gate variant, a gradient oscillating at $\omega_a \pm \delta$ with $\delta \ll \omega_a$ excites the center-of-mass motion of the electron crystal along the axial direction if the electrons are in the same spin state, i.e., $|\uparrow\uparrow\rangle$ or $|\downarrow\downarrow\rangle$. If the electrons are in the $|\uparrow\downarrow\rangle$ or $|\downarrow\uparrow\rangle$ state, the net force vanishes and the electron-center-of-mass (COM) motion is not excited. The corresponding Hamiltonian in the interaction picture is given by [36,37]

$$\hat{H} = \hbar\Omega_R(\hat{I}\otimes\hat{\sigma}_z + \hat{\sigma}_z\otimes\hat{I})(\hat{a}e^{-i\delta t} + \hat{a}^\dagger e^{i\delta t}), \qquad (2)$$

where Ω_R is the two-qubit gate Rabi frequency, $\hat{a}$ is the motional mode lowering operator, and σ_z is the Pauli operator. Because of the detuning δ of the force, the motion returns to its initial state for all four logical eigenstates after the gate time $t_{\text{gate}} = 2\pi/\delta$, enclosing an area in phase space. Different combinations of spin states acquire different geometrical phases, proportional to the area enclosed by their trajectories in phase space. For our parameters, the anticipated gate time for a two-qubit phase gate is about 2 μs.

For simplicity, we discussed the $\sigma_z \otimes \sigma_z$ gate, but $\sigma_x \otimes \sigma_x$ gates may offer certain advantages, as the drive is not near the motional frequency thereby suppressing unwanted excitation via residual electric fields. The $\sigma_z \otimes \sigma_z$ gate can also be implemented with all fields far detuned from the motional frequencies [11]. Such variants have been implemented using ions [38] with Bell-state fidelities $F = \text{Tr}(\rho_{\text{expt}}\rho_{\text{Bell}})$ reaching 99.7% [8], limited by motional heating and trap frequency instabilities, and 99.9% [11], limited mainly by motional dephasing, where ρ_{expt} and ρ_{Bell} are the density matrix operators of the experimentally prepared state and the ideal Bell-state intended to prepare, respectively.

III. ERROR SOURCES OF TWO-QUBIT GATES

High-fidelity gate operations are crucial for achieving fault-tolerant quantum computing. In the following, we use Bell-state fidelity as a proxy for operation fidelities and analyze the most important sources of gate infidelities for electron qubits in our trap configuration. Figure 3 shows an overview of the Bell-state infidelities $(1 - F)$ due to the most relevant decoherence sources (see Appendix C for details). Many of these error sources change slowly compared to the gate time and can be taken as quasistatic. This opens up the possibility of using dynamical decoupling sequences (for example, Walsh modulation) as used in state-of-the-art trapped-ion experiments [8,11,42,45–47], with a modest overhead in gate duration.

A. Motional heating

One of the dominant sources of error can be motional heating due to surface electric field noise. The motional heating rate is proportional to the electric-field spectral noise density $S(\omega_a)$ [14,48]:

$$\dot{n} = \frac{e^2}{4m_e\hbar\omega_a}S(\omega_a)\,. \qquad (3)$$

For a 30-μm ion-electrode distance, $S(\omega_a)$ near 1 MHz is expected to be approximately 10^{-12} V^2 m^2/Hz at cryogenic temperatures [48]. This corresponds to a heating rate of $\dot{n}_{\text{Ca}} = 100$ quanta/s at $\omega_a^{\text{Ca}} = 2\pi\times1$ MHz for Ca^+ ions. In order to extrapolate to gigahertz frequencies, we assume that the spectral noise density follows a power law $S(\omega_a) \propto 1/\omega_a^\gamma$. For ion traps, values of γ ranging from 1 to 1.5 have been measured [14,49–51]. Taking into account the light mass of electrons and an axial frequency of $\omega_a = 2\pi\times300$ MHz, the expected motional heating rate for electrons is

$$\dot{n}_e = \frac{m_{\text{Ca}}}{m_e}\left(\frac{\omega_a^{\text{Ca}}}{\omega_a}\right)^{1+\gamma}\dot{n}_{\text{Ca}}\,. \qquad (4)$$

For niobium traps at cryogenic temperatures, an exponent $\gamma = 1.3$ has been found [50], leading to an estimate for the heating rate of 14 quanta/s, which corresponds to a limit of the motional coherence time of 70 ms. Because of the uncertainties of extrapolation over two orders of magnitude in frequency, we conservatively assume a heating rate of 140 quanta/s, which yields a simulated Bell-state infidelity of about 8×10^{-5} with Walsh 3 modulation, as shown in the left panel of Fig. 3. For the transverse modes near 2 GHz, motional heating should be reduced by approximately two orders of magnitude to order 1 quantum/s.

B. Trap frequency instabilities

Instabilities of the trap frequency are caused by voltage noise, finite temperature of the electrons in combination with anharmonic potentials, as well as surface electric field noise.

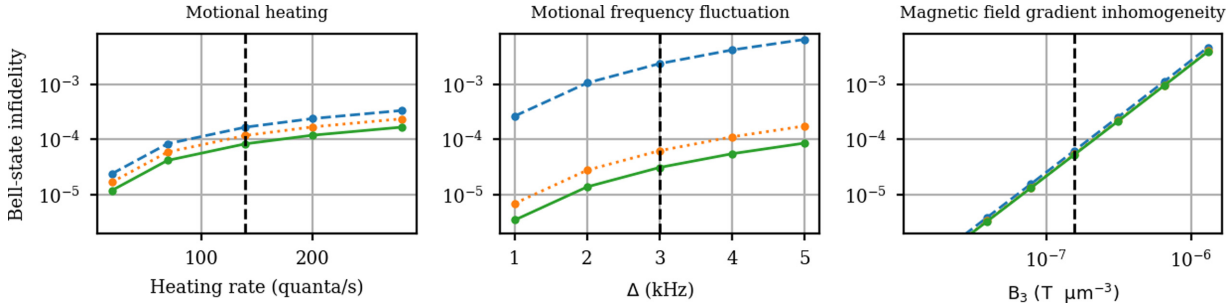

FIG. 3. Numerical simulation (QUTIP [44]) of three dominant error sources for an electron two-qubit gate. Blue dashed, orange dotted, and green solid curves correspond to no modulation, Walsh 1 modulation, and Walsh 3 modulation, respectively. For the magnetic field gradient inhomogeneity simulation, the three traces for different Walsh modulations overlap. To allow for an easy comparison, the y axis is the same on all three plots. Black dashed lines indicate our anticipated magnitude of the different error terms. Based on these error estimates, we estimate that the anticipated contribution to the Bell-state infidelity can be limited to 10^{-4} for all error sources considered here.

Trap frequency instabilities lead to a fluctuating detuning of the drive frequency from the motional sidebands at ω_a, and thereby to errors.

Formally, we distinguish between fast noise (dephasing) and slow noise (trap frequency fluctuations) as compared to a gate duration. Slow fluctuations can be mitigated effectively using modified phase-space trajectories [42,47,52–54]. Fast noise, on the other hand, cannot be easily mitigated other than by speeding up the quantum gates or by performing more loops in phase space.

Trap frequency fluctuations due to noise of the voltages applied to the electrodes are expected to be slow if low-pass filtered. Typical voltage sources provide fractional voltage stabilities on the order of 10^{-5}, corresponding to a motional frequency fluctuation $\Delta = 2\pi\times 3$ kHz. Using Walsh modulation one can suppress errors from slow frequency noise [52]. Assuming the above numbers, we estimate a residual Bell-state error of 3×10^{-5} with Walsh 3 modulation, as shown in the center panel of Fig. 3.

Finite electron temperatures lead to fluctuations in their oscillation periods due to the trap potential anharmonicities. Since motional heating is negligible over gate durations, this noise is also slow and can be taken care of by using Walsh modulations.

The quadrupole component of the surface electric field noise introduces noise to the quadrupole trapping potential, thereby causing fluctuations of the trap frequency. This noise component is related to the surface electric field noise as $S_Q(\omega_a) = \frac{15}{4d^2}S(\omega_a)$, where d is the electron-electrode distance, and $S(\omega_a)$ exhibits a $1/f^\alpha$ [55] characteristic with frequency scaling exponent $\alpha \gtrsim 1$, consisting of both fast and slow noise components, where f is the frequency of the noise. Reference [55] estimates that at $d \approx 25$ μm the integrated impact of quadrupole noise on the Bell-state fidelities is similar to that of motional heating. However, since the bulk electric field noise has a $1/f$ scaling, it can also be reduced by Walsh modulations.

In order to estimate the size of the fast noise, we draw on the insights of a recent ion trap experiment where for a trapping height of 30 μm its impact has been estimated to contribute 6×10^{-4} to the Bell-state infidelity [11,32]. The gate time in these experiments was several hundred microseconds, more than two orders of magnitude slower than what we expect for electrons. Thus, we expect that a significant amount of the fast noise observed in the ion trap experiments is actually slow in the context of electron quantum computing and can be removed with Walsh modulations. Assuming a $1/f$ characteristic, the remainder of the noise leads to a dephasing rate of $\Gamma = 2\pi\times1.8\times10^{-3}$ Hz, which corresponds to a Bell-state infidelity of 5×10^{-8}.

C. Inhomogeneity of the magnetic field gradient

The motional amplitude of trapped electrons at 0.4 K is a few hundreds of nanometers, which is large compared to $\sim$10 nm for ions. As a result, error sources usually not considered for trapped ions may become relevant. In particular, the electron experiences a variation of the force over the extent of its wavefunction, due to any inhomogeneity of the magnetic field gradient. Thus, for electron qubits, the homogeneity of the applied microwave radiation in combination with the finite electron temperature is relevant.

To estimate the lowest order effect of inhomogeneity, we do a Taylor expansion of the magnetic field, as discussed in Appendix C. Due to symmetry, the contribution of the second-order term (corresponding to the first-order term in magnetic field gradient ∇B) cancels over the extent of the electron motion. The third-order term (corresponding to the second-order term in ∇B), on the other hand, introduces a loss of fidelity due to a noncanceling force. Using the hairpin design shown in Fig. 1, we find the third-order expansion coefficient of the magnetic field to be $B_3 = 1.5\times10^{-7}$ T/μm^3, which causes an infidelity of 5×10^{-5} with Walsh 3 modulation (see the right panel of Fig. 3). Finally, we note that this effect can be reduced by reducing the temperature of the electrons as discussed in Appendix A.

D. Anharmonicity of the trapping potentials

The effect of the temperature on the COM mode frequency is given solely by the anharmonicity of the trapping potential itself. As discussed in Sec. II B, with the optimized trap potential up to the fourth order $V(z) = V(0)(1 + c_2z^2 + c_4z^4)$, we find $c_4/c_2 = 10^{-7}$ μm^{-2}, which corresponds to only very small contributions to the Bell-state infidelity and is on the order of 10^{-7} or below for Walsh modulations.

TABLE I. Estimates for the contribution of various error sources with Walsh 3 modulation.

	Motional heating	Trap frequency fluctuation	Motional dephasing	Magnetic field gradient inhomogeneity	Trapping potential anharmonicity	Qubit decoherence
Magnitude	140 quanta/s	3 kHz	1.8×10^{-3} Hz	1.5×10^{-7} T/μm^3	10^{-7} μm^{-2}	1 s
Infidelity	8×10^{-5}	3×10^{-5}	5×10^{-8}	5×10^{-5}	2×10^{-7}	3×10^{-6}

E. Qubit decoherence

The decoherence of the electron spin is expected to be dominated by magnetic field noise. Using magnetic shielding, coherence times of 300 ms (2 s with a spin echo) have been observed for Zeeman qubits in ions [56]. The greatly reduced optical overhead requirements for electron qubits as compared to the experiment in Ref. [56] will allow for more efficient magnetic shielding, leading to expected spin-coherence times in excess of 1 s without spin echo. This corresponds to only small contributions to Bell-state infidelities on the order of 3×10^{-6}.

In laser-free trapped-ion entangling gates, qubit frequency shift error can be suppressed effectively in a dynamically decoupled Mølmer-Sørensen gate [8] and $\sigma_z \otimes \sigma_z$ gate with intrinsic dynamical decoupling [11]. We expect a similar performance for electron qubits.

F. Summary of decoherence sources

In summary, we find that the largest source of infidelities will likely be magnetic field gradient inhomogeneities and motional heating, both expected to lead to errors smaller than 10^{-4} as shown in Table I. While these infidelities meet some commonly assumed error correction thresholds, they can be improved further. For instance, surface treatments may reduce motional heating [50] and thus suppress one of the largest error sources. Another path towards reducing motional heating would be to increase the electron-electrode distance. However, this will compromise achievable magnetic field gradients and motional frequencies.

IV. MODULARIZATION AND QUBIT ADDRESSING

A modular approach is preferred for constructing a large-scale quantum computer, and the most promising strategy for scaling trapped electron systems is adapting the quantum charge-coupled device (QCCD) architecture from trapped ions [5,6,57]. Since the trap frequencies for electrons we consider are approximately two orders of magnitude larger than typical values for trapped ions, we expect that electron transport and operations such as splitting and merging of the electron crystals can be carried out substantially faster than on equivalent trapped ions QCCD architecture.

Combining two-qubit gates with shuttling operations, we imagine entangling two electrons at specific sites in the QCCD device. Shuttling and splitting operations on electron crystals can be used to isolate a selected pair of electrons in a region where a localized magnetic field gradient can be applied to perform gates. These processing sites, with current-carrying wires providing the necessary magnetic field gradient, would be on the order of 200 μm long to allow for high-fidelity single-qubit addressing. In addition, the trap frequency would serve as an important discriminating element. Thus, we expect that crosstalk for multiqubit gates can be even lower than that for single-qubit gates. The electrons could be more densely packed in dedicated storage regions and can be shuttled between these two types of regions in a conveyor-belt fashion, and junctions could connect different processing and storage units with each other on a two-dimensional (2D) grid to create large entangled states.

To build a modular electron quantum computer, coupling of remote electron qubits could be engineered with a high-impedance coplanar waveguide that distributes image currents between distant sites. In Ref. [24], the authors estimate such a coupling between two electrons to be on the order of 100 kHz, which is a significant improvement over current implementations of remote entanglement in trapped-ion systems [58,59].

V. CONCLUSION AND OUTLOOK

In summary, we have conducted a feasibility study of a trapped-electron quantum information processing platform and have discussed the experimental steps and potential challenges towards building such a device, including schemes for trapping, cooling, electronic detection, spin readout, and quantum gates of electrons.

Numerical simulations of quantum gates with electron qubits show that the largest sources of infidelities will likely be motional heating and magnetic field gradient inhomogeneities, both expected to lead to Bell-state preparation infidelities below 10^{-4}. This may meet the requirements for fault-tolerant quantum computing with reasonable overheads. This system can be scaled up and modularized by adapting the QCCD architecture similarly to trapped-ion systems, allowing for single-qubit addressing and isolation of multiqubit operations from bystander electrons. Therefore, the trapped-electron technology proposed here meets the DiVincenzo criteria [60] for the physical realization of a quantum computer.

In addition to applications to quantum information processing, the development of techniques to trap cold electrons in Paul traps may also directly impact other disciplines, such as plasma physics through the study of small cold plasma [61] and electron-positron interactions [62], and to serve as sensitive detectors of charges including millicharged dark matter [63,64].

ACKNOWLEDGMENTS

We acknowledge support from AFOSR through Grant No. FA9550-20-1-0162, and the NSF QLCI program through Grant No. OMA-2016245. Work by A.A. and H.H. was sponsored by the U.S. Department of Energy, Office of Science,

Office of Basic Energy Sciences under Award No. DE-SC0019376. Q.Y., K.M.B., and R.T.S. acknowledge funding from the Lawrence Livermore National Laboratory (LLNL) Laboratory Directed Research and Development (LDRD) program under Grant No. 21-FS-008. Work done by K.M.B. was performed under the auspices of the U.S. Department of Energy by Lawrence Livermore National Laboratory under Contract No. DE-AC52-07NA27344. B.H. and M.D. would like to acknowledge support from the UC Laboratory Fees Research Program LFR-20-653698. K.J.R. acknowledges support from NSF GRFP.

APPENDIX A: THERMAL LOADS ON A CRYOGENIC TRAP

The model system we consider in Fig. 1 is assumed to reside in a cryogenic environment at 4 K with the resonant cooling circuit, as discussed further below, to be held at 0.4 K.

The most dominant heat source for the cryogenic electron trap is Joule heating from the current-carrying wires and AC electrodes. To determine the heat load on the 4-K stage, we assume that the current-carrying wires going from a 30-K stage to the 4-K stage are made of niobium with a length of 10 cm, a diameter of 1 mm, electrical resistivity of 1.5 nΩ m at 30 K, and thermal conductivity of 10 W/(m K) at 4 K. From this we estimate the heat load on the AC electrodes to be $\approx$4.5 mW per 1 A of current at 300 MHz with a duty cycle of $\approx$10% and $\approx$250 mW per 1 A of current at 10 GHz. More important will be the heat load from Joule dissipation in the AC electrodes themselves, which is directly transferred to the substrate. Assuming AC gradient electrodes with a cross section of $10\times0.5\ \mu\text{m}^2$ and a total length of 5 mm operating with a duty cycle of $\approx$10% for spin readout and gates, the estimated heat load is $\approx$100 mW per 1 A of current for copper with a specific resistance of $\approx$1 nΩ m and skin depth of $\approx0.9\,\mu$m at 4 K, 300 MHz. Regarding the AC trapping electrodes, assuming a drive voltage of 14 V at 10 GHz, and a capacitance of 1 pF, this will lead to a current of 1 A. Assuming further that the current flows through the entire AC copper electrode of length 5 mm, cross section $50\times0.5\ \mu\text{m}^2$, and a skin depth of $\approx0.16\ \mu$m, we arrive at a heat load $I^2R = 600$ mW per AC electrode pair, i.e., 1.2 W for all four. This heat load can be mitigated by providing a sufficiently large heat sink to a typical cryopulse-tube cooler with 1.8 W of cooling power at 4 K by carefully choosing the trap substrate with high heat conductivity (e.g., sapphire) and trap mounting materials.

In order to reach 0.4 K in the motion of the trapped electron, the resonant circuit must be cryogenically cooled to the same temperature. This can be done by thermally anchoring the resonant circuit at 0.4 K and connecting it to the pickup electrodes at 4 K with a Nb (niobium) wire. The wire needs to be a good electrical conductor and a good thermal insulator to ensure that the heat load of the trap on the resonant circuit is lower than the maximum cooling power of the 0.4-K stage, $\approx$1.4 mW. Coupling the resonant circuit with a Nb wire of 1 cm length and 100 μm diameter, the heat load on the resonant circuit is $\approx150\ \mu$W, which is within the cooling capacity of a commercial dilution refrigerator with a maximum cooling power of $\approx$1.4 mW.

APPENDIX B: STRONG DRIVE IN MOTION DETECTION

The amplifiers needed to detect the electron signal are prone to saturation due to the strong AC drive of the electron trap. To estimate the degree of filtering necessary to successfully detect an electron in the presence of the 10-GHz drive, we model the electron as a Johnson-noise source with a bandwidth of 1 MHz at 4 K corresponding to a noise power of -142 dBm, where the bandwidth is determined by the coupling of the electron to the tank circuit. Assuming a dynamic range of the amplifier of 70 dB, the pick up at the drive frequency at $\sim$10 GHz must be smaller than -70 dBm. We estimate that the power required to drive the trap will be of order 1 W (30 dBm), requiring an effective filtering of 100 dB.

First, we note that the signal is not applied to the detection circuit. Second, the resonant circuit picking up the signal from the electron itself serves as a filter: the trap drive is many gigahertz detuned from the resonant circuit's narrow resonance at $2\pi\times300$ MHz. Further, the amplifier itself will be optimized to amplify the 300-MHz signal rather than the high-frequency drive. Finally, we can filter the signal of $\sim$300 MHz, either via low-pass filter or, if that is still not sufficient, with another resonant circuit.

APPENDIX C: QUANTUM GATE SIMULATION

The Bell-state fidelity is defined as

$$F = \text{Tr}(\rho_{\text{expt}}\,|\Psi_{\text{Bell}}\rangle\,\langle\Psi_{\text{Bell}}|), \tag{C1}$$

where $|\Psi_{\text{Bell}}\rangle$ is the state vector of the ideal targeted Bell state and ρ_{expt} is the reduced density matrix of the total system tracing out the motional degree of freedom. The Bell-state infidelity is calculated as $1-F$.

Gate dynamics are simulated with the Lindblad master equation using QUTIP [44]:

$$\dot{\rho}(t) = -\frac{i}{\hbar}[\hat{H},\rho] + \sum_n \left[\hat{L}_n\rho\hat{L}_n^\dagger - \frac{1}{2}\rho\hat{L}_n^\dagger\hat{L}_n - \frac{1}{2}\hat{L}_n^\dagger\hat{L}_n\rho\right] \tag{C2}$$

where $\hat{L}_n$ is a Lindblad operator, $\hat{H} = \hat{H}_g + \hat{H}_e$ is the total Hamiltonian consisting of the gate dynamics $\hat{H}_g$ and possible error sources described by $\hat{H}_e$.

The gate Hamiltonian is described as

$$\hat{H}_g = \hbar\Omega_R(\hat{I}\otimes\hat{\sigma}_z + \hat{\sigma}_z\otimes\hat{I})(\hat{a}e^{-i\delta t} + \hat{a}^\dagger e^{i\delta t}), \tag{C3}$$

where Ω_R is the two-qubit gate Rabi frequency.

Motional heating. Motional heating is modeled with the Lindblad operators $L_1 = \sqrt{\gamma}\hat{a}$ and $L_2 = \sqrt{\gamma}\hat{a}^\dagger$, where $\gamma = \dot{n}_e$ is the motional heating rate, and $\hat{a}^\dagger$ and $\hat{a}$ are the creation and annihilation operators of the motional mode, respectively.

Motional frequency fluctuation. Motional frequency fluctuations are modeled with the Hamiltonian

$$\hat{H}_e = \hbar\Delta\hat{a}^\dagger\hat{a}, \tag{C4}$$

where Δ is the motional frequency detuning from ω_a.

Motional dephasing. Motional dephasing is modeled with the Lindblad operator $L_3 = \sqrt{\Gamma}\hat{a}^\dagger\hat{a}$, where Γ is the dephasing rate of the electron motion.

Inhomogeneity of the magnetic field gradient. Taylor expanding the magnetic field around the center of mass of the two-electron crystal, $B = B_0 + B_1 z + B_2 z^2 + B_3 z^3$, where B_j denotes the jth-order expansion coefficient of the magnetic field. Keeping only the slowly oscillating terms rotating with δ, the magnetic field gradient inhomogeneity error is modeled with the Hamiltonian [65]:

$$\hat{H}_e = 3\hbar\Omega_{\text{in}}(\hat{I}\otimes\hat{\sigma}_z + \hat{\sigma}_z\otimes\hat{I})(\hat{a}\hat{a}^\dagger\hat{a}e^{-i\delta t} + \hat{a}^\dagger\hat{a}\hat{a}^\dagger e^{i\delta t}), \quad \text{(C5)}$$

where $\Omega_{\text{in}} = \Omega_R \times 3z_0^2 B_3/B_1$, and z_0 is the ground-state extension of the axial motional mode.

Anharmonicity of the trapping potentials. Expanding the trapping potential to only the fourth order, $V(z) = V(0)(1 + c_2 z^2 + c_4 z^4)$, the trap potential anharmonicity can be modeled with the Hamiltonian

$$\hat{H}_e = V_4 \hat{z}^4 = V(0) c_4 z_0^4 (\hat{a}_z + \hat{a}_z^\dagger)^4. \quad \text{(C6)}$$

Qubit decoherence. Qubit decoherence is modeled with the Lindblad operator $\hat{L}_4 = \sqrt{\frac{1}{2\tau_{\text{spin}}}}\hat{\sigma}_z$, where τ_{spin} is the spin coherence time.

APPENDIX D: ELECTRON TRAJECTORY STABILITY

The electron trajectory stability is analyzed by numerically integrating the two-dimensional electron motion along radial directions. Since the surplus ionization energy is small compared to the potential energy in the trapping potential, we assume the initial kinetic energy of electrons to be zero. The simulation variables are the phase ϕ of the AC drive at the ionization time ($t = 0$) assuming a time dependence of $U_0 \cos(\omega_{\text{ac}} t + \phi)$ and the initial energy of electrons in the AC trapping potential which is determined by the ionization distance from the trap center. Figure 4 shows the simulation result, which is a map of the electron storage time simulated up to 100 μs. From the simulation, electron trajectories are not lost over the duration of the simulation for initial energies less than $k_{\text{B}} \times 250$ K which corresponds to an ionization distance of about 8 μm from the trap center. For higher energies, the stability of the electron trajectory depends strongly on the phase of the AC drive, and electron trajectories are the most stable when the phase of the AC electric field is zero when the electron is separated from its parent atom.

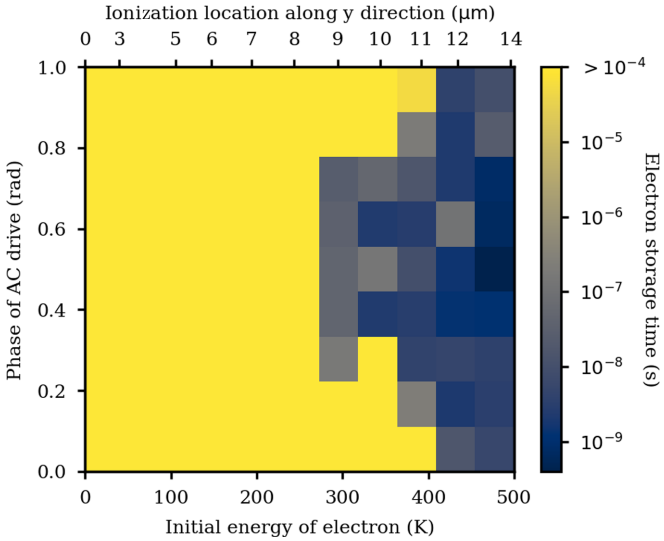

FIG. 4. Electron trajectory simulation of the two-dimensional secular motion. Electron trajectories are stable irrespective of the drive phase when the electron separates from the atom for initial energies less than 250 K.

[1] K. Mølmer and A. S. Sørensen, Multiparticle Entanglement of Hot Trapped Ions, Phys. Rev. Lett. **82**, 1835 (1999).

[2] J. Bollinger, D. Heinzen, W. Itano, S. Gilbert, and D. Wineland, A 303-MHz frequency standard based on trapped Be^+ ions, IEEE Trans. Instrum. Meas. **40**, 126â128 (1991).

[3] P. T. H. Fisk, M. J. Sellars, M. A. Lawn, and C. Coles, Accurate measurement of the 12.6 GHz Clock transition in trapped $^{171}Yb^+$ ions, IEEE Trans. Ultrason. Ferroelectr. Freq. Control **44**, 344 (1997).

[4] P. Wang, C.-Y. Luan, M. Qiao, M. Um, J. Zhang, Y. Wang, X. Yuan, M. Gu, J. Zhang, and K. Kim, Single ion qubit with estimated coherence time exceeding one hour, Nat. Commun. **12**, 233 (2021).

[5] D. Kielpinski, C. Monroe, and D. J. Wineland, Architecture for a large-scale ion-trap quantum computer, Nature (London) **417**, 709 (2002).

[6] D. J. Wineland, C. Monroe, W. M. Itano, D. Leibfried, B. E. King, and D. M. Meekhof, Experimental issues in coherent quantum-state manipulation of trapped atomic ions, J. Res. Natl. Inst. Stand. Technol. **103**, 259 (1998).

[7] T. P. Harty, D. T. C. Allcock, C. J. Ballance, L. Guidoni, H. A. Janacek, N. M. Linke, D. N. Stacey, and D. M. Lucas, High-Fidelity Preparation, Gates, Memory, and Readout of a Trapped-Ion Quantum Bit, Phys. Rev. Lett. **113**, 220501 (2014).

[8] T. P. Harty, M. A. Sepiol, D. T. C. Allcock, C. J. Ballance, J. E. Tarlton, and D. M. Lucas, High-Fidelity Trapped-Ion Quantum Logic Using Near-Field Microwaves, Phys. Rev. Lett. **117**, 140501 (2016).

[9] C. J. Ballance, T. P. Harty, N. M. Linke, M. A. Sepiol, and D. M. Lucas, High-Fidelity Quantum Logic Gates Using Trapped-Ion Hyperfine Qubits, Phys. Rev. Lett. **117**, 060504 (2016).

[10] J. P. Gaebler, T. R. Tan, Y. Lin, Y. Wan, R. Bowler, A. C. Keith, S. Glancy, K. Coakley, E. Knill, D. Leibfried, and D. J. Wineland, High-Fidelity Universal Gate Set for $^9Be^+$ Ion Qubits, Phys. Rev. Lett. **117**, 060505 (2016).

[11] R. Srinivas, S. C. Burd, H. M. Knaack, R. T. Sutherland, A. Kwiatkowski, S. Glancy, E. Knill, D. J. Wineland, D. Leibfried, A. C. Wilson, D. T. C. Allcock, and D. H. Slichter, High-fidelity laser-free universal control of trapped ion qubits, Nature (London) **597**, 209 (2021).

[12] K. K. Mehta, C. Zhang, M. Malinowski, T.-L. Nguyen, M. Stadler, and J. P. Home, Integrated optical multi-ion quantum logic, Nature (London) **586**, 533 (2020).

[13] R. J. Niffenegger, J. Stuart, C. Sorace-Agaskar, D. Kharas, S. Bramhavar, C. D. Bruzewicz, W. Loh, R. T. Maxson, R. McConnell, D. Reens, G. N. West, J. M. Sage, and J. Chiaverini, Integrated multi-wavelength control of an ion qubit, Nature (London) **586**, 538 (2020).

[14] K. R. Brown, J. Chiaverini, J. M. Sage, and H. Häffner, Materials challenges for trapped-ion quantum computers, Nat. Rev. Mater. **6**, 892 (2021).

[15] N. C. Brown and K. R. Brown, Comparing Zeeman qubits to hyperfine qubits in the context of the surface code: $^{174}Yb^{+}$ and $^{171}Yb^{+}$, Phys. Rev. A **97**, 052301 (2018).

[16] P. Bushev, S. Stahl, R. Natali, G. Marx, E. Stachowska, G. Werth, M. Hellwig, and F. Schmidt-Kaler, Electrons in a cryogenic planar Penning trap and experimental challenges for quantum processing, Eur. Phys. J. D **50**, 97 (2008).

[17] I. Marzoli, P. Tombesi, G. Ciaramicoli, G. Werth, P. Bushev, S. Stahl, F. Schmidt-Kaler, M. Hellwig, C. Henkel, G. Marx, I. Jex, E. Stachowska, G. Szawiola, and A. Walaszyk, Experimental and theoretical challenges for the trapped electron quantum computer, J. Phys. B: At. Mol. Opt. Phys. **42**, 154010 (2009).

[18] J. Goldman and G. Gabrielse, Optimized planar Penning traps for quantum-information studies, Phys. Rev. A **81**, 052335 (2010).

[19] S. A. Lyon, Spin-based quantum computing using electrons on liquid helium, Phys. Rev. A **74**, 052338 (2006).

[20] G. Yang, A. Fragner, G. Koolstra, L. Ocola, D. A. Czaplewski, R. J. Schoelkopf, and D. I. Schuster, Coupling an Ensemble of Electrons on Superfluid Helium to a Superconducting Circuit, Phys. Rev. X **6**, 011031 (2016).

[21] G. Koolstra, G. Yang, and D. I. Schuster, Coupling a single electron on superfluid helium to a superconducting resonator, Nat. Commun. **10**, 5323 (2019).

[22] E. Kawakami, A. Elarabi, and D. Konstantinov, Image-Charge Detection of the Rydberg States of Surface Electrons on Liquid Helium, Phys. Rev. Lett. **123**, 086801 (2019).

[23] X. Zhou, G. Koolstra, X. Zhang, G. Yang, X. Han, B. Dizdar, D. Ralu, W. Guo, K. W. Murch, D. I. Schuster, and D. Jin, Electron on solid neon—a new solid-state single-electron qubit platform, arXiv:2106.10326.

[24] N. Daniilidis, D. J. Gorman, L. Tian, and H. Hartmut, Quantum information processing with trapped electrons and superconducting electronics, New J. Phys. **15**, 073017 (2013).

[25] P. Peng, C. Matthiesen, and H. Häffner, Spin readout of trapped electron qubits, Phys. Rev. A **95**, 012312 (2017).

[26] S. Kotler, R. W. Simmonds, D. Leibfried, and D. J. Wineland, Hybrid quantum systems with trapped charged particles, Phys. Rev. A **95**, 022327 (2017).

[27] C. Matthiesen, Q. Yu, J. Guo, A. M. Alonso, and H. Häffner, Trapping Electrons in a Room-Temperature Microwave Paul Trap, Phys. Rev. X **11**, 011019 (2021).

[28] D. J. Wineland and H. G. Dehmelt, Principles of the stored ion calorimeter, J. Appl. Phys. **46**, 919 (1975).

[29] L. S. Brown and G. Gabrielse, Geonium theory: Physics of a single electron or ion in a Penning trap, Rev. Mod. Phys. **58**, 233 (1986).

[30] D. J. Gorman, P. Schindler, S. Selvarajan, N. Daniilidis, and H. Häffner, Two-mode coupling in a single-ion oscillator via parametric reson ance, Phys. Rev. A **89**, 062332 (2014).

[31] S. C. Burd, R. Srinivas, J. J. Bollinger, A. C. Wilson, D. J. Wineland, D. Leibfried, D. H. Slichter, and D. T. Allcock, Quantum amplification of mechanical oscillator motion, Science **364**, 1163 (2019).

[32] S. C. Burd, R. Srinivas, H. M. Knaack, W. Ge, A. C. Wilson, D. J. Wineland, D. Leibfried, J. J. Bollinger, D. T. Allcock, and D. H. Slichter, Quantum amplification of boson-mediated interactions, Nat. Phys. **17**, 898 (2021).

[33] D. J. Wineland, P. Ekstrom, and H. Dehmelt, Monoelectron Oscillator, Phys. Rev. Lett. **31**, 1279 (1973).

[34] E. A. Cornell, R. M. Weisskoff, K. R. Boyce, and D. E. Pritchard, Mode coupling in a Penning trap: π pulses and a classical avoided crossing, Phys. Rev. A **41**, 312 (1990).

[35] S. Sturm, A. Wagner, B. Schabinger, and K. Blaum, Phase-Sensitive Cyclotron Frequency Measurements at Ultralow Energies, Phys. Rev. Lett. **107**, 143003 (2011).

[36] C. F. Roos, Ion trap quantum gates with amplitude-modulated laser beams, New J. Phys. **10**, 013002 (2008).

[37] D. Leibfried, B. DeMarco, V. Meyer, D. Lucas, M. Barrett, J. Britton, W. M. Itano, B. Jelenković, C. Langer, T. Rosenband, and D. J. Wineland, Experimental demonstration of a robust, high-fidelity geometric two ion-qubit phase gate, Nature (London) **422**, 412 (2003).

[38] C. Ospelkaus, U. Warring, Y. Colombe, K. R. Brown, J. M. Amini, D. Leibfried, and D. J. Wineland, Microwave quantum logic gates for trapped ions, Nature (London) **476**, 181 (2011).

[39] F. Mintert and C. Wunderlich, Ion-Trap Quantum Logic Using Long-Wavelength Radiation, Phys. Rev. Lett. **87**, 257904 (2001).

[40] C. Ospelkaus, C. E. Langer, J. M. Amini, K. R. Brown, D. Leibfried, and D. J. Wineland, Trapped-Ion Quantum Logic Gates Based on Oscillating Magnetic Fields, Phys. Rev. Lett. **101**, 090502 (2008).

[41] R. Srinivas, S. C. Burd, R. T. Sutherland, A. C. Wilson, D. J. Wineland, D. Leibfried, D. T. C. Allcock, and D. H. Slichter, Trapped-Ion Spin-Motion Coupling with Microwaves and a Near-Motional Oscillating Magnetic Field Gradient, Phys. Rev. Lett. **122**, 163201 (2019).

[42] A. E. Webb, S. C. Webster, S. Collingbourne, D. Bretaud, A. M. Lawrence, S. Weidt, F. Mintert, and W. K. Hensinger, Resilient Entangling Gates for Trapped Ions, Phys. Rev. Lett. **121**, 180501 (2018).

[43] H. Hahn, G. Zarantonello, M. Schulte, A. Bautista-Salvador, K. Hammerer, and C. Ospelkaus, Integrated $^{9}Be^{+}$ multi-qubit gate device for the ion-trap quantum computer, npj Quantum Inf. **5**, 70 (2019).

[44] J. Johansson, P. Nation, and F. Nori, QuTiP: An open-source Python framework for the dynamics of open quantum systems, Comput. Phys. Commun. **183**, 1760 (2013).

[45] T. Manovitz, A. Rotem, R. Shaniv, I. Cohen, Y. Shapira, N. Akerman, A. Retzker, and R. Ozeri, Fast Dynamical Decoupling of the Mølmer-Sørensen Entangling Gate, Phys. Rev. Lett. **119**, 220505 (2017).

[46] R. T. Sutherland, R. Srinivas, S. C. Burd, D. Leibfried, A. C. Wilson, D. J. Wineland, D. T. Allcock, D. H. Slichter, and S. B. Libby, Versatile laser-free trapped-ion entangling gates, New J. Phys. **21**, 33033 (2019).

[47] R. T. Sutherland, R. Srinivas, S. C. Burd, H. M. Knaack, A. C. Wilson, D. J. Wineland, D. Leibfried, D. T. C. Allcock, D. H. Slichter, and S. B. Libby, Laser-free trapped-ion entangling gates with simultaneous insensitivity to qubit and motional decoherence, Phys. Rev. A **101**, 042334 (2020).

[48] M. Brownnutt, M. Kumph, P. Rabl, and R. Blatt, Ion-trap measurements of electric-field noise near surfaces, Rev. Mod. Phys. **87**, 1419 (2015).

[49] D. A. Hite, Y. Colombe, A. C. Wilson, K. R. Brown, U. Warring, R. Jördens, J. D. Jost, K. S. McKay, D. P. Pappas, D. Leibfried, and D. J. Wineland, 100-Fold Reduction of Electric-Field Noise in an Ion Trap Cleaned with In Situ Argon-Ion-Beam Bombardment, Phys. Rev. Lett. **109**, 103001 (2012).

[50] J. A. Sedlacek, J. Stuart, D. H. Slichter, C. D. Bruzewicz, R. McConnell, J. M. Sage, and J. Chiaverini, Evidence for multiple mechanisms underlying surface electric-field noise in ion traps, Phys. Rev. A **98**, 063430 (2018).

[51] C. Noel, M. Berlin-Udi, C. Matthiesen, J. Yu, Y. Zhou, V. Lordi, and H. Häffner, Electric-field noise from thermally activated fluctuators in a surface ion trap, Phys. Rev. A **99**, 063427 (2019).

[52] D. Hayes, S. M. Clark, S. Debnath, D. Hucul, I. V. Inlek, K. W. Lee, Q. Quraishi, and C. Monroe, Coherent Error Suppression in Multiqubit Entangling Gates, Phys. Rev. Lett. **109**, 020503 (2012).

[53] F. Haddadfarshi and F. Mintert, High fidelity quantum gates of trapped ions in the presence of motional heating, New J. Phys. **18**, 123007 (2016).

[54] Y. Shapira, R. Shaniv, T. Manovitz, N. Akerman, and R. Ozeri, Robust Entanglement Gates for Trapped-Ion Qubits, Phys. Rev. Lett. **121**, 180502 (2018).

[55] I. Talukdar, D. J. Gorman, N. Daniilidis, P. Schindler, S. Ebadi, H. Kaufmann, T. Zhang, and H. Häffner, Implications of surface noise for the motional coherence of trapped ions, Phys. Rev. A **93**, 043415 (2016).

[56] T. Ruster, C. T. Schmiegelow, H. Kaufmann, C. Warschburger, F. Schmidt-Kaler, and U. G. Poschinger, A long-lived Zeeman trapped-ion qubit, Appl. Phys. B **122**, 254 (2016).

[57] B. Lekitsch, S. Weidt, A. G. Fowler, K. Mølmer, S. J. Devitt, C. Wunderlich, and W. K. Hensinger, Blueprint for a microwave trapped ion quantum computer, Sci. Adv. **3**, e1601540 (2017).

[58] D. Hucul, I. V. Inlek, G. Vittorini, C. Crocker, S. Debnath, S. M. Clark, and C. Monroe, Modular entanglement of atomic qubits using photons and phonons, Nat. Phys. **11**, 37 (2014).

[59] L. J. Stephenson, D. P. Nadlinger, B. C. Nichol, S. An, P. Drmota, T. G. Ballance, K. Thirumalai, J. F. Goodwin, D. M. Lucas, and C. J. Ballance, High-Rate, High-Fidelity Entanglement of Qubits Across an Elementary Quantum Network, Phys. Rev. Lett. **124**, 110501 (2020).

[60] D. P. DiVincenzo, The physical implementation of quantum computation, Fortschr. Phys. **48**, 771 (2000).

[61] K. A. Twedt and S. L. Rolston, Electronic Detection of Collective Modes of an Ultracold Plasma, Phys. Rev. Lett. **108**, 065003 (2012).

[62] J. R. Danielson, D. H. E. Dubin, R. G. Greaves, and C. M. Surko, Plasma and trap-based techniques for science with positrons, Rev. Mod. Phys. **87**, 247 (2015).

[63] D. Carney, H. Häffner, D. C. Moore, and J. M. Taylor, Trapped Electrons and Ions as Particle Detectors, Phys. Rev. Lett. **127**, 061804 (2021).

[64] D. Budker, P. W. Graham, H. Ramani, F. Schmidt-Kaler, C. Smorra, and S. Ulmer, Millicharged dark matter detection with ion traps, arXiv:2108.05283.

[65] R. T. Sutherland, Q. Yu, K. M. Beck, and H. Häffner, One- and two-qubit gate infidelities due to motional errors in trapped ions and electrons, arXiv:2111.01913.